Ring opening reaction dynamics in the reaction of hydrogen atoms with ethylene oxide

S. K. Shin and R. L. Jarek
Department of Chemistry, University of California, Santa Barbara, Santa Barbara, California 93106

E. Böhmer[a)] and C. Wittig
Department of Chemistry, University of Southern California, Los Angeles, California 90089-0482

(Received 4 April 1994; accepted 1 July 1994)

Ethylene oxide, C_2H_4O, is a three-membered ring with a single oxygen atom bridging the two carbons. Reactions of H and D atoms with ethylene oxide have been studied in the gas phase to provide insight into the dynamics of three-membered ring opening. H atoms were produced by photolyzing HI in the wavelength range 240–266 nm. The channel leading to $OH+C_2H_4$ was monitored via laser-induced fluorescence (LIF) of the OH $A\,^2\Sigma \leftarrow X\,^2\Pi$ system. The D atom reaction yields OD with no hydrogen scrambling. With an available energy of 23 000 cm^{-1}, the average OH D rotational energy is ~350 cm^{-1} for OH($v=0$) and OD($v=0$) and ~250 cm^{-1} for OD($v=1$). OH($v=1$) was not observed, while the OD($v=1$) population was about one-tenth that of OD($v=0$). There was no apparent bias in populations between Λ doublets in each of the spin–orbit states for both OH and OD. Doppler broadening of OH($v=0$) rotational lines was measured to evaluate the average center-of-mass (c.m.) translational energy, which was found to be ~2300 cm^{-1}. On average, the ring opening process deposits ~10% of the available energy into c.m. translation, ~2% into OH rotation, and ~88% into ethylene internal energy. Comparison with CH_2CH_2OH unimolecular dissociation dynamics and theoretical transition state calculations leads to a likely mechanism in which hydrogen abstracts oxygen via sequential C–O bond fission without involving a long-lived CH_2CH_2OH intermediate.

I. INTRODUCTION

Bimolecular reactions of fast hydrogen atoms with small molecules have been studied extensively for the purpose of elucidating the corresponding reaction dynamics at the state-to-state level.[1,2] Typically, these atoms are prepared by using HX (hydrogen halide) photodissociation, which yields translational energies that are high enough to overcome barriers to reaction.[1] The photon energy defines the total available energy, and the hydrogen atoms can have two speeds, corresponding to the two halogen spin–orbit levels. This technique has been applied to reactions with H_2,[3,4] D_2,[5] O_2,[6] CO_2,[7] N_2O,[8] OCS,[9] and H_2O.[10,11] In all cases, the incident hydrogen removes one of the terminal atoms, sometimes via a vibrationally excited intermediate, and detailed dynamical information has been obtained from product state distributions[12] as well as from product buildup times.[13] However, there are presently no experimental reports concerning the dynamics of ring opening.

In the work reported here, the state-selective pump–probe technique has been applied to the study of ring opening reaction dynamics. Measurements are reported for reactions of hydrogen atoms with ethylene oxide, C_2H_4O, yielding $OH+C_2H_4$. Ethylene oxide was chosen because it is a three-membered ring compound (the oxygen atom bridges the carbons) with electronic absorption bands below 212 nm, i.e., the $A \leftarrow X$ transition lies in the region 212–160 nm.[14] Thus, the system can be examined by photodissociating HX throughout the convenient wavelength range 220–270 nm without electronically exciting the ethylene oxide. In the present experiments, hydrogen was produced by 240–266 nm HI photodissociation and the OH product was observed by using laser-induced fluorescence (LIF). State-specific OH detection provides information about energy partitioning among product degrees of freedom as well as information about the propensity for orbital alignment in the OH product.[15]

In the present experiments, fast hydrogen atoms approach ethylene oxide with no geometrical bias, thus creating several possibilities. When attacking oxygen, OH can be formed by breaking two bridging C–O bonds concurrently. Alternatively, an O–H bond can be formed while breaking a C–O bond to form the CH_2CH_2OH intermediate, which subsequently dissociates to $OH+C_2H_4$ or to $H+CH_2CHOH$. When attacking carbon, a C–H bond can be formed while breaking an adjacent C–O or C–C bond. C–O bond rupture leads to formation of the CH_3CH_2O radical intermediate, which dissociates to CH_3+H_2CO or to $H+CH_3CHO$. Hydrogen migration in CH_3CH_2O can lead to the CH_2CH_2OH intermediate, thereby scrambling the hydrogens. C–C bond cleavage yields the CH_3OCH_2 radical intermediate, which dissociates to CH_3+H_2CO.

Fast incident hydrogen may also strip hydrogen from ethylene oxide yielding H_2+CH_2CHO. Because of the high available energy, the CH_2CHO product can in principle fragment to $OH+C_2H_2$, even though the overall enthalpy change is +21 kcal mol^{-1}. However, this will be shown to be unimportant by experiments that measure hydrogen scrambling.

Reactive pathways for processes having negative enthalpy changes are listed below.

a)Present address: Science Center, Rockwell International Corporation, 1049 Camino Dos Rios, Thousand Oaks, CA 91360.

 0021-9606/94/101(8)/6615/10/$6.00

			ΔH (kcal mol^{-1})	
$H+C_2H_4O$	$\rightarrow OH+C_2H_4$		−18.3,	(1)
	$\rightarrow CH_2CH_2OH$		−47.0,	(2)
	$\rightarrow CH_2CH_2OH$	$\rightarrow OH+C_2H_4$	−18.3,	(3)
		$\rightarrow H+CH_2CHOH$	−17.4,	(4)
	$\rightarrow H+CH_2CHOH$		−17.4,	(5)
	$\rightarrow H+CH_3CHO$		−27.5,	(6)
	$\rightarrow CH_3CH_2O$		−42.3,	(7)
	$\rightarrow CH_3CH_2O$	$\rightarrow H+CH_3CHO$	−27.5,	(8)
		$\rightarrow CH_3+H_2CO$	−31.4,	(9)
	$\rightarrow CH_3OCH_2$		−48.9,	(10)
	$\rightarrow CH_3OCH_2$	$\rightarrow CH_3+H_2CO$	−31.4.	(11)

The heats of formation that were used to evaluate the above enthalpy changes are listed in Table I. Though many channels are possible, only OH is observed in the present study. This species can be produced by reactions (1) and (3) as well as the hydrogen migration channels:

$$CH_3CH_2O^{\dagger}\rightarrow CH_2CH_2OH^{\dagger}\rightarrow OH+C_2H_4, \quad (12)$$

$$CH_2CH_2OH^{\dagger}\rightarrow CH_2CH_2O^{\dagger}\rightarrow CH_2CH_2OH^{\dagger}\rightarrow OH+C_2H_4. \quad (13)$$

To test for migration, experiments were carried out with fast deuterium atoms while monitoring OH and OD. Specifically, the detection of OH would provide direct evidence for migration. None was found.

Though reactions (1) and (3) yield the same products, they differ mechanistically. Consequently, the dynamics of these reactions may differ qualitatively, and this can be reflected in product state distributions and buildup times. For example, if ring opening has a sizable entrance barrier and the total energy is large relative to any wells encountered in the overall process, bias may be seen in OH produced via reaction (1). Alternatively, a vibrationally excited, long-lived $CH_2CH_2OH^{\dagger}$ intermediate can be expected to decompose via a unimolecular reaction mechanism.

Lee and co-workers carried out photofragment translational spectroscopic studies of 2-bromoethanol at 193 nm.[16] They found that it dissociates to atomic bromine and CH_2CH_2OH, some of which subsequently decomposes to $OH+C_2H_4$ due to the internal excitation it receives in the primary photodissociation process. Translational energy distributions were obtained for products, including long-lived CH_2CH_2OH intermediates that survived for 100–200 μs. More recently, Sapers and Hess characterized OH deriving from $CH_2CH_2OH^{\dagger}$ decomposition, following the 202 nm photodissociation of 2-bromoethanol. The nascent $CH_2CH_2OH^{\dagger}$ from 2-bromoethanol photodissociation contains enough internal energy to decompose. They also photodissociated 2-iodoethanol at 266 nm,[17] obtaining OH state distributions from the secondary photodissociation of CH_2CH_2OH, as inferred from fluence dependence measurements. In this case, the OH rotational distribution extended to $N''=15$ and displayed broad Doppler profiles.

Since dynamics are sensitive to the entrance channel barrier and wells encountered in the overall process, structural and energetic information about the transition state and intermediate is valuable in interpreting the data. For example, the reverse reaction of OH with ethylene has been studied theoretically by Sosa and Schlegel.[18,19] Thus, we carried out *ab initio* calculations to find the transition state and activation barrier for the entrance channel.

TABLE I. Heats of formation at 0 K.[a,b]

Molecule	ΔH_{f0} (kcal mol^{-1})	Molecule	ΔH_{f0} (kcal mol^{-1})
H	51.6	CH_2CHOH	−27.0
D	52.5	CH_3CHO	−37.1
Ethylene oxide	−9.6	CH_3CH_2O	−0.3
OH	9.2	CH_3	35.6
OD	8.7	H_2CO	−25.0
C_2H_4	14.5	CH_3OCH_2	−6.9
CH_2CH_2OH [c]	−5.0		

[a]D. D. Wagman, W. H. Evans, V. B. Parker, R. H. Schumm, I. Halow, S. M. Bailey, K. L. Churney, and R. L. Nuttall, J. Phys. Chem. Ref. Data **11**, Suppl. 2 (1981).
[b]S. G. Lias, J. E. Bartmess, J. F. Liebman, J. L. Holmes, R. D. Levin, and W. G. Mallard, J. Phys. Chem. Ref. Data **17**, Suppl. 1 (1988).
[c]C. Sosa and H. B. Schlegel, J. Am. Chem. Soc. **109**, 7007 (1987).

II. EXPERIMENT

The experimental arrangement is essentially the same as that reported earlier in our study of photoinitiated reactions of hydrogen and deuterium atoms with N_2O.[8] However, ethylene oxide and HI(DI) can react heterogeneously, making it advisable to minimize the surface area in simultaneous contact with both gases. Each gas entered the chamber through a separate inlet, thereby eliminating effects due to heterogeneous processes. Reactions were examined with flowing samples of typically 50% oxirane and 50% HI(DI) at a total chamber pressure of 40 mTorr. The delay between the photolysis and probe lasers was optimized to give the best signal-to-noise ratio while ensuring nascent product distributions under single-collision, arrested-relaxation conditions. The photolysis probe delay was set typically at 100 ns. Under these conditions, products undergo ~0.1 hard sphere collisions.

Hydrogen atoms were prepared by pulsed laser HI photodissociation in the wavelength range 240 to 266 nm. The broad HI absorption spectrum[20] allows the photolysis wavelength to be varied considerably when using the doubled output of an excimer-pumped dye laser. Since HI photolysis yields I atoms in both the ground ($^2P_{3/2}$) and excited ($^2P_{1/2}$) states, hydrogen atoms are produced with two different translational energies.[20,21] However, as shown below, the lower translational energy does not contribute significantly to OH production and therefore will not be considered further. Thus, the reported OH(OD) populations reflect contributions mainly from the faster hydrogen atoms. Table II summarizes the average collision energies, collision energy spreads due to the thermal velocity distributions of the collision partners, and average energies available for product excitations.

Deuterium atoms were produced by 240 nm photolysis of DI to directly compare the OD and OH rotational distribution at the same total available energy. The average collision energy is given (for hydrogen) by

TABLE II. Average collision energy, collision energy spread, and energy available for product excitations in H-atom reactions with ethylene oxide.

Photolysis molecule	λ (nm)	$h\nu - D_0 + RT$ (cm^{-1})	$\langle E_{collision}\rangle$ (cm^{-1})	$\Delta E_{collision}$ (cm^{-1})	$\langle E_{available}\rangle$ (cm^{-1})
HI	243.5	16 639	16 142	1055	22 935
HI	266.4	13 110	12 719	938	19 512
DI	240.0	16 708	15 734	1457	23 014

$$\langle E_{collision}\rangle = (44/45)(127/128)[h\nu - D_0(HI) + RT]. \quad (14)$$

The bond dissociation energies of HI and DI are 3.054 and 3.094 eV, respectively.[22] The RT term is the average HI(DI) rotational energy, which appears as translational energy following photolysis. The superthermal widths of the collision energy distributions are calculated from the expression derived by Chantry[23] and by van der Zande *et al.*[24] The available energy is given by the formula

$$\langle E_{available}\rangle + \langle E_{collision}\rangle + 3RT/2 + \langle E_{vib}(C_2H_4O)\rangle - \Delta H_0, \quad (15)$$

where $3RT/2$ is the average ethylene oxide rotational energy, $\langle E_{vib}(C_2H_4O)\rangle$ is the average ethylene oxide vibrational energy at 300 K (80 cm^{-1}), and ΔH_0 is the reaction enthalpy change.

Nascent OH(D) distributions were obtained via LIF by using the $A\ ^2\Sigma \leftarrow X\ ^2\Pi$ system in the region 306–317 nm. The dependence of the LIF signal on the probe fluence was examined carefully to check for saturation on several transitions having large Einstein B coefficients. Saturation was avoided by using probe energies ≤ 1 μJ with a 4 mm diameter spot. Typically the photolysis beam was focused to a 3 mm diameter spot with energies of 60 μJ to 1 mJ, corresponding to fluences of 0.8–14 mJ cm^{-2}. However, the OH LIF signal was not checked for photolysis fluence dependence. Interestingly, in the photodissociation of 2-iodoethanol, Sapers and Hess have observed that CH_2CH_2OH absorbs at 266 nm, yielding OH for fluences ~1 mJ cm^{-2}. This resulted in an OH rotational distribution with N'' as high as 15 and broad Doppler profiles. Since the photolysis fluences in our experiments are typically ≥ 1 mJ cm^{-2}, CH_2CH_2OH, if formed within the photolysis pulse, may absorb a photon, yielding an OH rotational distribution comparable to that observed by Sapers and Hess. However, this will be a minor channel in the present experiments because only a small percentage of the reactive collisions occur during the photolysis pulse. In addition, we photolyzed HI at 250.8 nm and DI at 308 nm to produce hydrogen and deuterium atoms with the same linear momentum. For 308 nm DI photolysis, no OD signal was observed, presumably because of the small absorption cross section and/or the low collision energy (21 kcal mol^{-1}), which is comparable to the calculated entrance barrier of 19 kcal mol^{-1}.

Ethylene oxide (99.7%) was obtained from Liquid Carbonic and was used without further purification. Hydrogen iodide (Matheson, 98% minimum) and deuterium iodide (Cambridge Isotope Laboratories, 99%) were used without further purification.

A. Computational details

Geometries were optimized with valence double-ζ basis sets for carbon $(9s5p/3s2p)$ and oxygen $(9s5p/3s2p)$, augmented with one set of d-polarization functions for carbon and oxygen [$\zeta^d(C)=0.75$ and $\zeta^d(O)=0.85$].[25] Scaled double-ζ basis sets (scale factor of 1.2) were used for hydrogen $(4s/2s)$ augmented with one set of p functions [$\zeta^p(H)=1.00$].[25] Total energies for stationary points along the reaction path were calculated with triple-ζ basis sets for carbon $(10s6p/5s3p)$ and oxygen $(10s6p/5s3p)$, augmented with two sets of d-polarization functions for carbon and oxygen [$\zeta^d(C)=1.940$, 0.409 and $\zeta^d(O)=1.477$, 0.531].[26,27] Scaled triple-ζ basis sets (scale factor of 1.2) were used for hydrogen $(6s/3s)$ augmented with two sets of p functions [$\zeta^p(H)=1.517$, 0.659].[26,27] The present basis sets for the hydrogen atom yield a total energy of 0.499 705 hartree.

The entrance channel was followed by gradually moving the hydrogen close to the oxygen and optimizing geometrical parameters with a fixed hydrogen–oxygen distance at the unrestricted Hartree–Fock (UHF) second-order Møller–Plesset perturbation (UMP2) level.[28] For the transition state, a transition state search routine available in the GAUSSIAN 92

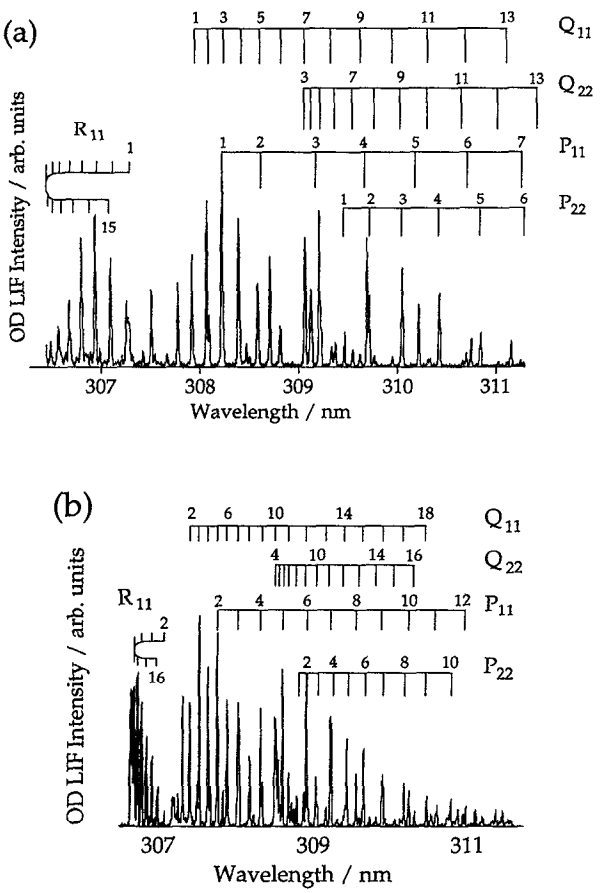

FIG. 1. (a) OH($v=0$) LIF spectra for bulk conditions; 243.5 nm HI photodissociation. Only the main OH($v=0$) rotational branches are assigned. (b) OD($v=0,1$) LIF spectra for bulk conditions; 240 nm DI photodissociation. Only the main OD($v=0$) rotational branches are assigned.

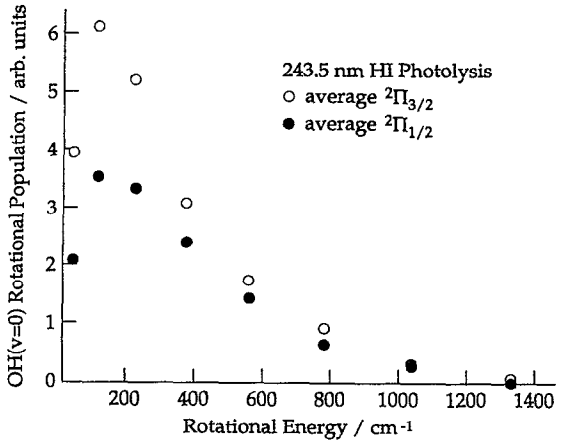

FIG. 2. OH($v=0$) rotational level distributions for bulk conditions; 243.5 nm HI photolysis. Open circles represent the average of the F_1 levels ($^2\Pi_{3/2}$). Filled circles represent the average of the F_2 levels ($^2\Pi_{1/2}$).

program was used.[29] Since the UHF wave function is not an eigenfunction of the spin, we have also used spin-projected energies (PMP2) corrected to first order for spin contamination in the UMP2 wave function.[18,19,30] We have also employed the restricted open-shell Hartree–Fock (ROHF) second-order Møller–Plesset perturbation (ROMP2) method[31] to correctly estimate the activation barrier without spin contamination in the wave function with a UMP2-optimized transition state geometry. Transition state frequencies were obtained at the UMP2 level. Geometries for ethylene oxide and CH_2CH_2OH were optimized at the MP2 level.

III. RESULTS

Representative parts of OH and OD LIF spectra are shown in Fig. 1 for 300 K bulk samples under single-collision, arrested-relaxation conditions. Signals were normalized for sample pressure and photolysis and probe fluences. To obtain OH(OD) rotational distributions, the normalized spectra were fitted to simulated spectra obtained by the convolution of the experimentally measured line shape with the known line positions and strengths. OH(OD) radiative lifetimes were also taken into account.[32,33]

Rotational distributions of OH($v=0$) for 243.5 nm HI photolysis are shown in Fig. 2. Within experimental limits, OH($v=1$) was not detected. The ratio of spin–orbit populations is $[^2\Pi_{1/2}]/[^2\Pi_{3/2}]\sim 0.6$ for OH($v=0$). No apparent bias was observed for Λ-doublet populations, indicating no preferential alignment of the singly occupied orbital with respect to the plane of rotation for the higher N'' values.[15] The rotational distribution of OH($v=0$) peaks at $N''=2$ for both spin–orbit states with little population above $N''=8$. When the total available energy was reduced from 23 000 to 19 400 cm^{-1} by changing the photolysis wavelength from 243.5 to 266.4 nm, the OH rotational distribution did not change appreciably. Figure 3 shows OH($^2\Pi_{3/2}$, $v=0$) Boltzmann plots for 243.5 and 266.4 nm HI photolyses.

When DI was photolyzed at 240 nm to give the same total available energy as 243.5 nm HI photolysis, no OH hydrogen scrambling product was observed within the experimental detection limits. This is direct evidence against hydrogen migration. Rotational distributions for OD($v=0$) and OD($v=1$) are shown in Fig. 4. Bias against the higher $^2\Pi_{1/2}$ spin–orbit level is apparent, while no bias in the Λ-doublet populations was detected. The ratio of spin–orbit populations is $[^2\Pi_{1/2}]/[^2\Pi_{3/2}]\sim 0.5$ and 0.2 for OD($v=0$) and OD($v=1$), respectively. The OD($v=0$) rotational distribution peaks at $N''=3$ for both spin–orbit states, with little population above $N''=12$, while that of OD($v=1$) peaks at $N''=1$ or 2 for both spin–orbit states, with little population above $N''=6$. Boltzmann plots of the $^2\Pi_{3/2}$ levels of OD($v=0$) and OD($v=1$) are shown in Fig. 5.

When the available energy was the same for HI and DI photolyses (i.e., approximately 23 000 cm^{-1}), the OH and

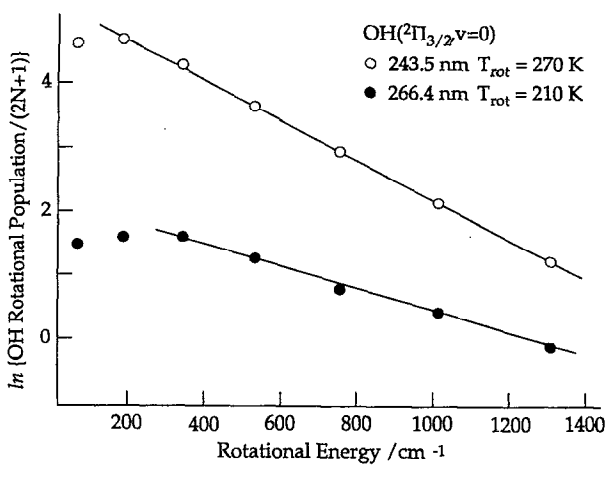

FIG. 3. Boltzmann plots for OH($^2\Pi_{3/2}$, $v=0$) rotational level distributions. Open circles denote the 243.5 nm photolysis. Filled circles denote the 266 nm photolysis.

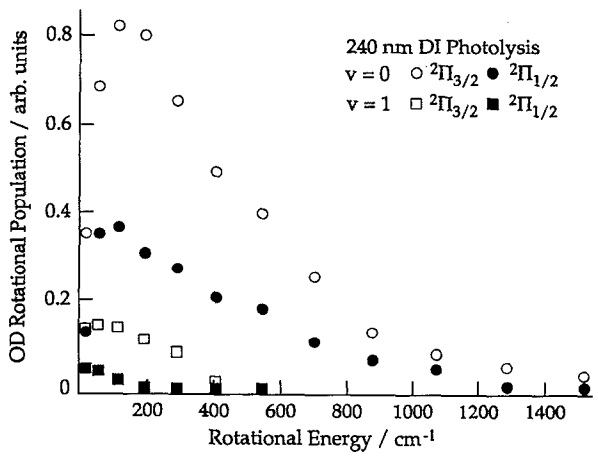

FIG. 4. OD rotational distributions for bulk conditions; 240 nm DI photodissociation. Circles denote OD($v=0$), while squares denote OD($v=1$). Open symbols represent the average of the F_1 levels ($^2\Pi_{3/2}$). Filled symbols represent the average of the F_2 levels ($^2\Pi_{1/2}$).

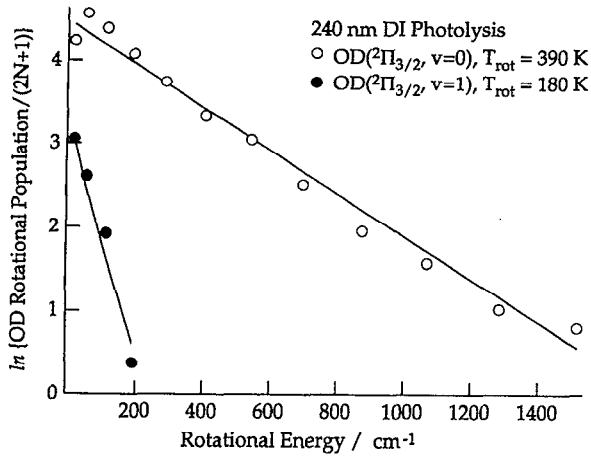

FIG. 5. Boltzmann plots for OD($^2\Pi_{3/2}$) rotational level distributions obtained from P_{11} rotational lines of OD in the 240 nm DI photodissociation. Open circles represent OD($^2\Pi_{3/2}$, $v=0$) and filled circles represent OD($^2\Pi_{3/2}$, $v=1$). Rotational temperatures were assigned to the linear parts of distributions.

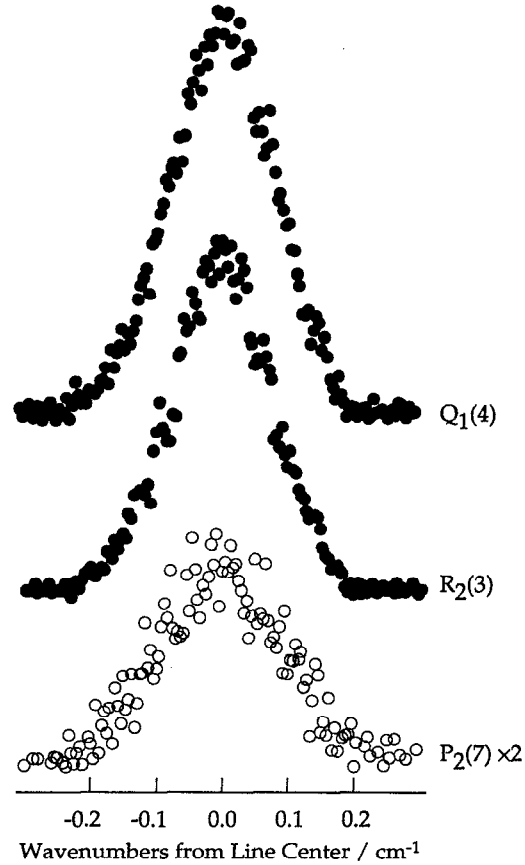

FIG. 6. OH sub-Doppler LIF spectra for bulk conditions; 243.5 nm HI photodissociation. The linewidth of the probe laser was ~0.08 cm^{-1}. Spectra for $P_2(7)$, $R_2(3)$, and $Q_1(4)$ rotational lines show the similar Doppler broadening independent of the rotational quantum number, the rotational branch, and the spin–orbit level probed.

OD rotational distributions revealed almost identical biases in the spin–orbit and Λ-doublet populations. Both OH($v=0$) and OD($v=0$) have average rotational energies of ~350 cm^{-1}. Considering the available energy of approximately 23 000 cm^{-1}, OH rotations are very cold. The only noticeable difference between the hydrogen and deuterium reactions is that deuterium produces OD($v=1$). OD($v=1$) has an average rotational energy of ~250 cm^{-1}. Predissociation of OD($A\ ^2\Sigma$) with $v\geq2$ precludes interrogation of $v>1$. However, the OD $[v=1]/[v=0]$ ratio of ~0.1 suggests that there is probably little population above $v=1$.

Since OH and OD have little internal excitation, most of the available energy resides in product degrees of freedom such as c.m. translation and ethylene internal excitation. To help clarify the energy partitioning, product translation was examined by observing the Doppler effect on OH line shapes. Unpolarized 243.5 nm photolysis radiation was used, and profiles were monitored for different *P*, *Q*, and *R* branches and for different N'' values. No significant changes in line shapes or widths were observed for the different rotational branches and quantum numbers. Representative Doppler profiles for $P_2(7)$, $Q_1(4)$, and $R_2(3)$ are shown in Fig. 6. For a given distribution, the average OH translational energy was found to be 1400±300 cm^{-1} with a maximum translational energy of 8400±1700 cm^{-1}, corresponding to average and maximum c.m. translational energies of 2300 ±500 and 13 500±2700 cm^{-1}, respectively. This is low considering that the excess energy is approximately 23 000 cm^{-1}, and that the OH($v=0$) levels being monitored have modest internal energy. This means that the ethylene fragment associated with the probed OH levels has an average internal energy of ~20 000 cm^{-1}.

IV. DISCUSSION

When hydrogen atoms react with ethylene oxide to yield OH there is no scrambling of the incident and ethylene hydrogens. This is consistent with reactions (1) and/or (3). To further establish the mechanism, structural and energetic information was obtained from *ab initio* calculations, while dynamical information was obtained from the present experiments and from previous studies of CH_2CH_2OH unimolecular decomposition.

A. Transition state and potential energy

Table III lists total energies for the transition state and CH_2CH_2OH. It also lists the total energy for H+ethylene oxide at the transition state H–O distance of 1.2375 Å without relaxing the ethylene oxide geometry. This provides an estimate of the dynamical activation barrier. Since relative energies for reactants, products, and CH_2CH_2OH are available in the literature, the transition state energy was compared with that of CH_2CH_2OH. The energy difference between the UMP2 optimized transition state and CH_2CH_2OH is 72.0 kcal mol^{-1} at the UMP2 level, 71.1 kcal mol^{-1} at the PMP2 level, and 71.8 kcal mol^{-1} at the ROMP2 level. With the PMP2 optimized transition state, the energy difference is 71.7 kcal mol^{-1} at the UMP2 level, 71.7 kcal mol^{-1} at the PMP2 level, and 72.2 kcal mol^{-1} at the ROMP2 level. If

TABLE III. Total energies (hartree) and energy differences (kcal mol^{-1}) for the transition state and CH_2CH_2OH with the triple-ζ plus double polarization basis set; geometries were optimized with the double-ζ plus single polarization basis set.

	Level				
Geometry	UHF	UMP2	PMP2	ROHF	ROMP2
UMP2 optimized transition state	−153.354 377	−153.904 682	−153.908 149	−153.348 931	−153.905 334
R(H–O)=1.2375 Å	(S^2=0.783)			(S^2=0.750)	
ΔE (kcal mol^{-1})	97.9	72.0	71.1	98.5	71.8
PMP2 optimized transition state	−153.359 320	−153.905 053	−153.907 139	−153.355 743	−153.904 694
R(H–O)=1.245 Å	(S^2=0.768)			(S^2=0.750)	
ΔE (kcal mol^{-1})	94.8	71.7	71.7	94.3	72.2
H+ethylene oxide	−153.366 321	−153.901 747	−153.902 610	−153.364 405	−153.901 431
R(H–O)=1.2375 Å	(S^2=0.756)			(S^2=0.750)	
ΔE (kcal mol^{-1})	90.4	73.8	74.5	88.8	74.3
CH_2CH_2OH	−153.510 404	−154.019 372	−154.021 411	−153.505 952	−154.019 783
	(S^2=0.762)			(S^2=0.750)	

CH_2CH_2OH is used as an anchor point in the estimation of the transition state barrier, the transition state lies 19.1 kcal mol^{-1} above the reactants at the UMP2 level after correcting for zero-point energies. Transition state frequencies are listed in Table IV. The zero-point energy for the transition state is 37.4 kcal mol^{-1}. The zero-point energy of 43.3 kcal mol^{-1} for CH_2CH_2OH was taken from the theoretical result of Sosa and Schlegel.[18] The dynamical activation barrier is found to lie only 1.8 kcal mol^{-1} above the UMP2 optimized transition state barrier at the UMP2 level.

Figure 7 shows a potential energy diagram for H+ethylene oxide going to $OH+C_2H_4$. Hydrogen atoms that attack the bridging oxygen face an entrance barrier of approximately 19 kcal mol^{-1}. The CH_2CH_2OH intermediate lies 47 kcal mol^{-1} below the reactants, while $OH+C_2H_4$ lies 28.7 kcal mol^{-1} above CH_2CH_2OH. There is no barrier in the exit channel; the exit channel barrier has been calculated to lie 0.9 kcal mol^{-1} below the products by Sosa and Schlegel.[19] Figure 8 shows geometries for several stationary points along the reaction path. Ethylene oxide has C–O distances of 1.443 Å and a C–C distance of 1.476 Å at the MP2 level. The entrance channel transition state has an H–O distance of 1.238 Å at the UMP2 level and 1.245 Å at the PMP2 level. The C–O distance in the entrance channel transition state is 1.601 Å, which is 0.158 Å extended from the reactant ethylene oxide, and the C–C distance in the transition state is 1.448 Å, which is 0.028 Å contracted from the reactant. It is noteworthy that *ethylene oxide retains its symmetrical geometry at the transition state indicating an early transition state in the ring opening reaction.*

TABLE IV. Transition state vibrational frequencies and zero-point energy.

Frequency (cm^{-1})	Zero-point energy (kcal mol^{-1})
2504*i*, 3364, 3348, 3238, 3230, 1575, 1506, 1274, 1229, 1145, 1041, 960, 954, 937, 823, 743, 444, 382	37.4

The CH_2CH_2OH intermediate has an O–H distance of 0.967 Å, a C–O distance of 1.431 Å, and a C–C distance of 1.497 Å, optimized at the UMP2 level. The exit channel transition state has an O–H distance of 0.954 Å, a C–O distance of 1.925 Å, and a C–C distance of 1.393 Å, optimized at the HF/6-31G* level.[19] The product O–H distance is 0.970 Å and the C–C distance in ethylene is 1.339 Å. Thus, the C–C bond contracts from 1.476 Å in ethylene oxide to 1.448 Å in the transition state, extends to 1.497 Å in the CH_2CH_2OH intermediate, contracts back to 1.393 Å at the exit channel transition state, and forms a C–C double bond of 1.339 Å in ethylene. Once past the entrance barrier, ring opening may prefer the path in which the C–C bond gets progressively shorter over the path that first elongates the C–C bond to form the CH_2CH_2OH intermediate.

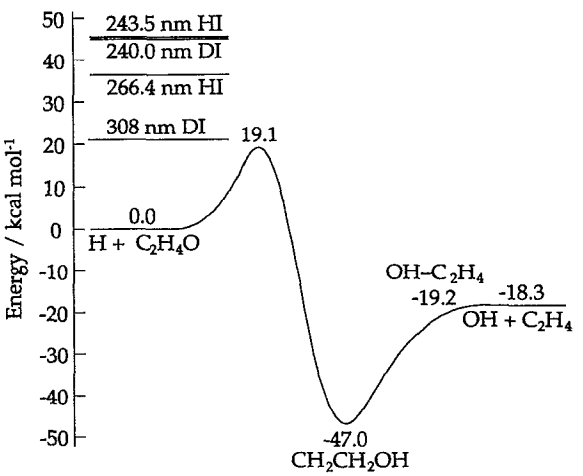

FIG. 7. Potential energy diagram for the H+ethylene oxide system producing $OH+C_2H_4$. Energies are in units of kcal mol^{-1}.

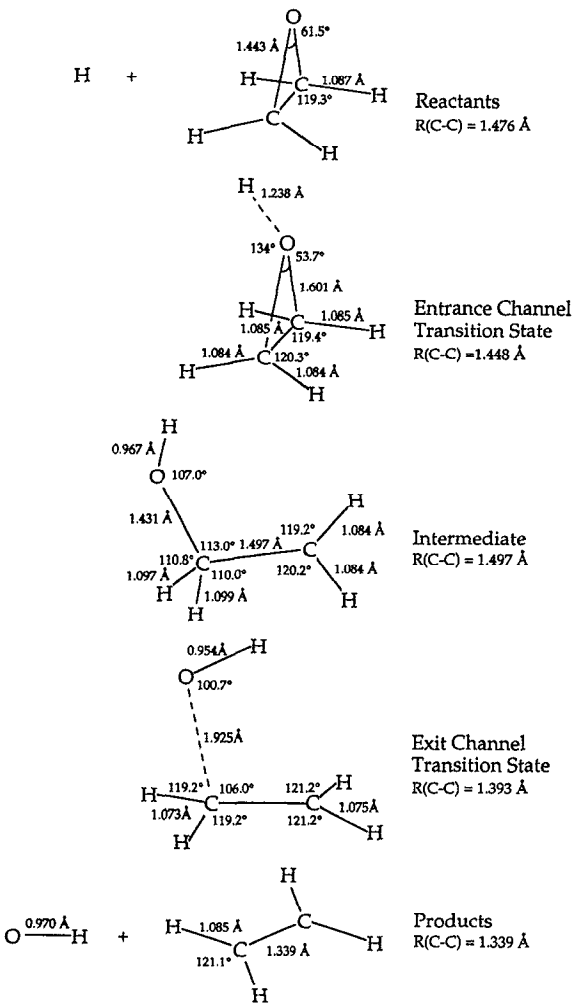

FIG. 8. Geometries for stationary points along the path shown in Fig. 7. Note that numbers derive from different sources, so comparisons between structures require care.

B. Energy distributions

In the case of 243.5 nm HI photolysis, the energy available for product excitations is approximately 23 000 cm^{-1}. The average OH rotational excitation is ~350 cm^{-1}, and within the experimental detection limit no vibrational excitation was observed. The average OH translational energy is 1400±300 cm^{-1} and the maximum OH translational energy is 8400±1700 cm^{-1}. These correspond to average and maximum c.m. translational energies of 2300±500 and 13 500 ±2700 cm^{-1} in the c.m. system, respectively. Thus, ethylene possesses an average internal energy of ~20 000 cm^{-1}. Since this is less than the lowest triplet energy (22 100 cm^{-1}) and the internal rotational barrier (22 800 cm^{-1}),[34] we assume this energy is mostly vibrational, including internal rotation.

To further characterize the dynamics, a rotational prior distribution was calculated for OH($v=0$).[35,36] The result is shown in Fig. 9. Ethylene was treated as a symmetric top[37] and its vibrations were taken to be harmonic. CH vibrations

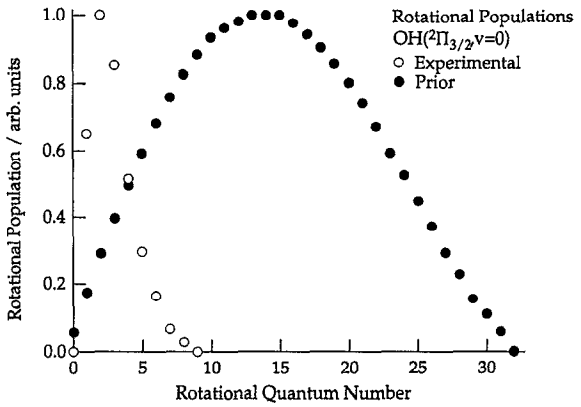

FIG. 9. The rotational level distribution for OH($^2\Pi_{3/2}$, $v=0$) from a prior calculation (filled circles) in comparison with the experimental results (open circles) from the 243.5 nm HI photodissociation.

are more anharmonic than the lower frequency vibrations but contribute less to the state sums. The experimental result is *much* colder than the prior distribution. Because there is no exit channel barrier, if ring opening involves a long-lived CH_2CH_2OH intermediate, product excitations can be quite statistical. The most probable rotational quantum number from the experiment is $N''=3$; from the prior it is $N''=15$. This large difference argues against the long-lived CH_2CH_2OH intermediate.

The nonstatistical product distribution is probably due to a short ring opening time. Consequently, the excitation of certain ethylene vibrations was estimated by calculating Franck–Condon (FC) factors for projections of the C_2H_4 moiety in either ethylene oxide or the entrance channel transition state onto the ethylene product. These FC factors are $|\langle\Psi|v\rangle|^2$, where $|\Psi\rangle$ is the vibrational wave function for ethylene oxide or the transition state and $|v\rangle$ is for ethylene. Vibrations were taken to be harmonic; the parameters used in the calculations are listed in Table V. The C–C stretching force constant for ethylene was taken from the valence force field given by Herzberg.[37] Force constants for ethylene oxide and the transition state were estimated by using a frequency–force constant relationship.[38] Figure 10 shows these FC factors vs C–C stretch vibrational quantum number. They peak at $v=1$ and 2 for the transition state and ethylene oxide, respectively. The average vibrational energy deposited in the C–C stretch is ~2910 cm^{-1} for the transition state and ~3790 cm^{-1} for ethylene oxide. Structural differences be-

TABLE V. Parameters for harmonic wave functions used in the C–C stretch Franck–Condon overlap calculation.

	Ethylene	Ethylene oxide	Transition state
ν (cm^{-1})	1623	1271	1159[a]
k (mdyn $Å^{-1}$)	9.57	5.87[b]	4.88[b]
$\alpha=k/h\nu$ ($Å^{-2}$)	296.6	232.4	211.8
r_e(C–C) (Å)	1.339	1.464	1.448

[a]Scaled (0.91) from the calculated frequency of 1274 cm^{-1}.
[b]Estimated by using the equation $k=(\nu/\nu_{\text{ethylene}})^2\, k_{\text{ethylene}}$.

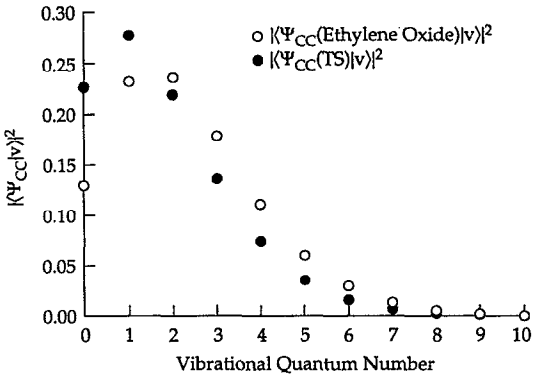

FIG. 10. Franck–Condon factors for the C–C stretch vibration. Open circles represent overlaps between ethylene oxide and ethylene. Filled circles represent overlaps between the transition state and ethylene.

tween ethylene oxide and ethylene also suggest excitation of CH_2 bending modes: ν_7=949 cm^{-1} and ν_8=943 cm^{-1}.[37] The FC factors vs CH_2 bending vibrational quantum number are shown in Fig. 11; they peak at $v=1$. The average vibrational energies in ν_7 and ν_8 are each ~1030 cm^{-1}. Thus, the average vibrational energy deposited into the ν_2, ν_7, and ν_8 modes is ~5850 cm^{-1} in going from ethylene oxide to ethylene. Thus, the remaining 14 500 cm^{-1} is distributed among other nine vibrational degrees of freedom and the three ethylene rotational degrees of freedom.

To further establish the mechanism for ethylene internal excitation, ethylene total energies were calculated at the MP2 level with triple-ζ double polarization basis sets for the ethylene moieties in ethylene oxide, the entrance channel transition state, and the CH_2CH_2OH intermediate, as well as for free ethylene (see Fig. 8). The transition state ethylene lies 10.1 kcal mol^{-1} (3550 cm^{-1}) above free ethylene, while the oxide ethylene lies 16.1 kcal mol^{-1} (5630 cm^{-1}) above free ethylene. The energy difference of 5630 cm^{-1} is consistent with the average vibrational energy of 5850 cm^{-1} estimated from the FC factors in going from ethylene oxide to ethylene. This result indicates that vibrational excitation residing in the other degrees of freedom cannot account for the remaining 14 500 cm^{-1}. On the other hand, the CH_2CH_2OH radical ethylene lies 62.4 kcal mol^{-1} (21 800 cm^{-1}) above the equilibrium ethylene. This energy is close to the average internal energy of ~20 000 cm^{-1} in the ethylene product. Since the CH_2CH_2OH radical ethylene differs from others mainly by its 57.5° twisted CH_2 plane, the remaining 14 500 cm^{-1} is considered to be deposited into the CH_2 internal rotation in ethylene. This means that ring opening proceeds via sequential C–O bond fission rather than concerted simultaneous C–O bond breaking.

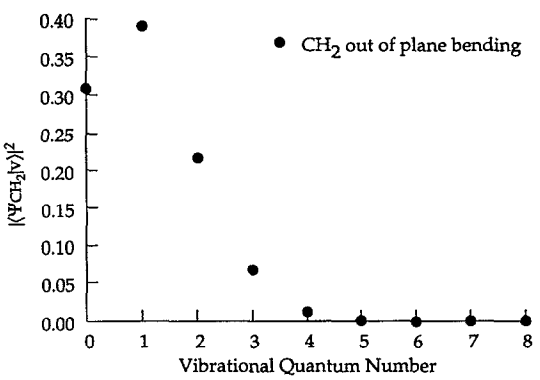

FIG. 11. Franck–Condon factors for the CH_2 out-of-plane bending vibration between ethylene oxide and ethylene.

Deuterium substitution affects product energy partitioning rather little even though deuterium moves more slowly than hydrogen. Both hydrogen and deuterium reactions produce internally cold OH and OD with modest c.m. translational energy and result in considerable internal excitation in ethylene. Since ring opening results from C–O bond fission, the energy partitioning in the ring opening products is mainly governed by the C–O bond fission process.

C. Comparisons with previous results

An important issue is whether OH is produced by direct abstraction or via an intermediate. To help settle this, the present results are compared with previous studies in which the CH_2CH_2OH intermediate is a known participant. Specifically, comparisons can be made with the unimolecular dissociation of CH_2CH_2OH effected by photolyzing $BrCH_2CH_2OH$. The unimolecular reaction of CH_2CH_2OH also involves significant structural changes: (i) the C–C distance changes from 1.497 Å in the radical to 1.339 Å in ethylene; (ii) the CH_2 planes twist by 57.5°; and (iii) two of the C–H distances change from 1.098 Å in the radical to 1.085 Å in ethylene.

Lee and co-workers obtained the c.m. translational energy distribution for the bromine atom as well as CH_2CH_2OH radicals that survived the flight time of 100–200 μs from the 2-bromoethanol photodissociation at 193 nm.[16] The total available energy is 81 kcal mol^{-1} and the observed upper and lower limits for the c.m. translational energy are 48 and 20 kcal mol^{-1}, respectively. This yields $CH_2CH_2OH^{\dagger}$, having a distribution of internal energies, whose average is ~47 kcal mol^{-1}. The CH_2CH_2OH flight time of $\geq$100 μs corresponds to $CH_2CH_2OH^{\dagger}$ unimolecular reaction rates $\leq 1\times10^4$ s^{-1}. To estimate the corresponding energies, unimolecular reaction rates were calculated by using an RRKM program with adiabatic rotation and Whitten–Rabinovitch approximations; the frequencies and threshold energy were taken from the calculations of Sosa and Schlegel.[18] The results are shown in Fig. 12. Rates $\leq 1\times10^4$ s^{-1} correspond to vibrational energies $\leq$28.7 kcal mol^{-1}. Thus, the observed translational energy distribution of the surviving CH_2CH_2OH radical is from highly rotationally excited CH_2CH_2OH.

Sapers and Hess reported two-step fragmentation of $BrCH_2CH_2OH$ following 202 nm photolysis.[17] The first step produces $Br+CH_2CH_2OH^{\dagger}$, the second step involves unimolecular decomposition of the nascent $CH_2CH_2OH^{\dagger}$ photoproduct, yielding $OH+C_2H_4$. $CH_2CH_2OH^{\dagger}$ internal energy distributions can be estimated from the photofragment time-

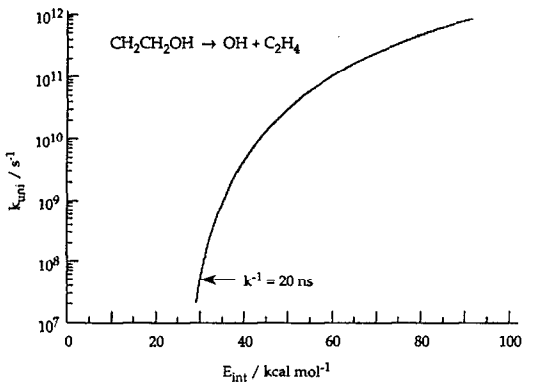

FIG. 12. RRKM reaction rates for the unimolecular dissociation of CH_2CH_2OH as a function of internal energy. Energies are in units of kcal mol^{-1}.

of-flight (TOF) results of Lee and co-workers.[16] The total available energy in the primary products is 74 kcal mol^{-1} and the upper and lower limits in the scaled c.m. translational energy are 44 and 18 kcal mol^{-1}, respectively. An average internal energy in $CH_2CH_2OH^{\dagger}$ is ~43 kcal mol^{-1}. Since Sapers and Hess monitored OH with a 20 ns photolysis probe delay, their observations were biased toward $CH_2CH_2OH^{\dagger}$ unimolecular reaction rates $\geqslant 5\times10^{7}s^{-1}$, which correspond to vibrational energies $\geqslant$~30 kcal mol^{-1}. Thus, Sapers and Hess observed unimolecular decomposition of highly vibrationally excited CH_2CH_2OH.

In the 243.5 nm HI photolysis experiment, the translational energy of the c.m. system is ~1 kcal mol^{-1}, which is 1/44 of the average collision energy, $\langle E_{\text{collision}}\rangle$. Reactions of H atoms with ethylene oxide can deposit an average internal energy of 93 kcal mol^{-1} into the CH_2CH_2OH radical, if formed. This is the sum of the average collision energy of 46 kcal mol^{-1} and the CH_2CH_2OH enthalpy of formation of 47 kcal mol^{-1}. The CH_2CH_2OH rotational energy is related to the collision energy:

$$E_{\text{rot}}=\frac{\mu b^2}{I}E_{\text{collision}}, \tag{16}$$

where μ is the reduced mass of the reactants, b is the entrance impact parameter, and I is the CH_2CH_2OH moment of inertia. With $\mu=0.978$ amu, $b=1.89$ Å (with H atom approaching the C_s symmetry transition state in a line perpendicular to the OCC plane) and $I=26.3$ amu Å^2, the CH_2CH_2OH rotational energy is ~6 kcal mol^{-1}. Thus, the vibrational energy in $CH_2CH_2OH^{\dagger}$ is ~87 kcal mol^{-1}. This is more than twice the average internal energy of 43 kcal mol^{-1} in the CH_2CH_2OH radical from the 202 nm photodissociation of 2-bromoethanol. The corresponding unimolecular reaction rate is 6.9×10^{11} s^{-1}. If CH_2CH_2OH lives long enough to undergo statistical unimolecular decomposition, the OH rotational distribution from highly vibrationally excited CH_2CH_2OH would be significantly hotter than that observed in the 2-bromoethanol photodissociation. To the contrary, the present results are colder, providing evidence against formation of long-lived CH_2CH_2OH.

In the 240 nm DI photolysis experiment, the average internal energy that can be deposited into the CH_2CH_2OD radical is 93.5 kcal mol^{-1}. With $\mu=1.913$ amu, $b=1.89$ Å, and $I=27.9$ amu Å^2 (the CH_2CH_2OD moment of inertia), the CH_2CH_2OD rotational energy is ~11 kcal mol^{-1}. Thus, the CH_2CH_2OD vibrational energy is ~82.5 kcal/mol. The corresponding unimolecular reaction rate is 5.2×10^{11} s^{-1}. Deuterium reactions proceed with more rotational excitation than H-atom reactions. If CH_2CH_2OD is formed, it would live longer than CH_2CH_2OH because of the higher rotational excitation and slower unimolecular reaction rate. Thus, the OD rotational distribution is expected to be more statistical than the OH rotational distribution. The observed OD rotational distribution is far from being more statistical.

The nonstatistical OH rotational distribution argues against the participation of a long-lived CH_2CH_2OH intermediate, though deuterium substitution favors formation of CH_2CH_2OD. To account for the cold OH(D) rotational distribution and high ethylene internal excitation, it is suggested that the O–H bond is formed as a C–O bond breaks; CH_2CH_2OH then dissociates without randomizing the internal energy.

V. CONCLUSIONS

Reactions of hydrogen and deuterium atoms with ethylene oxide reveal three-membered ring opening dynamics. OH(D) derives predominantly from the incident hydrogen; there is no indication of hydrogen scrambling. Ring opening occurs with little OH(D) rotational excitation and high internal excitation in ethylene. In light of *ab initio* theoretical transition state calculations combined with energy distributions and previous experimental results, it is suggested that the ring opening proceeds via direct oxygen abstraction through sequential C–O bond fission. However, ring opening occurs without involving a long-lived hydroxyethyl radical intermediate.

ACKNOWLEDGMENT

One of us (S.K.S.) thanks the University of California for a Regent's Junior Faculty Fellowship. Research supported by the U.S. National Science Foundation under Grant Nos. CHE-8822067 (C.W.) and CHE-9302959 (S.K.S).

[1] G. W. Flynn and R. E. Weston, Jr., Annu. Rev. Phys. Chem. **37**, 551 (1986).
[2] S. K. Shin, Y. Chen, S. Nickolaisen, S. W. Sharpe, R. A. Beaudet, and C. Wittig, in *Advances in Photochemistry*, edited by D. H. Volman, G. S. Hammond, and D. C. Neckers (Wiley, New York, 1991), Vol. 16, p. 249.
[3] J.-C. Nieh and J. J. Valentini, J. Chem. Phys. **92**, 1083 (1990).
[4] D. A. V. Kliner and R. N. Zare, J. Chem. Phys. **92**, 2107 (1990).
[5] E. E. Marinero, C. T. Rettner, and R. N. Zare, J. Chem. Phys. **80**, 4142 (1984).
[6] K. Kleinermanns and J. Wolfrum, J. Chem. Phys. **80**, 1446 (1984).
[7] Y. Chen, G. Hoffmann, D. Oh, and C. Wittig, Chem. Phys. Lett. **159**, 426 (1989).
[8] E. Böhmer, S. K. Shin, Y. Chen, and C. Wittig, J. Chem. Phys. **97**, 2536 (1992).
[9] E. Böhmer, K. Mikhaylichenko, and C. Wittig, J. Chem. Phys. **99**, 6545 (1993).
[10] K. Kessler and K. Kleinermanns, Chem. Phys. Lett. **190**, 145 (1992).
[11] R. B. Metz, J. D. Thoemke, J. M. Pfeiffer, and F. F. Crim, J. Chem. Phys. **99**, 1744 (1993).

[12] F. F. Crim, Annu. Rev. Phys. Chem. **44**, 397 (1993).
[13] S. Ionov, G. A. Brucker, C. Jaques, L. Valachovic, and C. Wittig, J. Chem. Phys. **99**, 6553 (1993).
[14] G. Herzberg, *Electronic Spectra and Electronic Structure of Polyatomic Molecules* (Van Nostrand Reinhold, New York, 1966).
[15] M. J. Bronikowski and R. N. Zare, Chem. Phys. Lett. **166**, 5 (1990).
[16] E. J. Hintsa, X. Zhao, and Y. T. Lee, J. Chem. Phys. **92**, 2280 (1990).
[17] S. P. Sapers and W. P. Hess, J. Chem. Phys. **97**, 3126 (1992).
[18] C. Sosa and H. B. Schlegel, J. Am. Chem. Soc. **109**, 7007 (1987).
[19] C. Sosa and H. B. Schlegel, J. Am. Chem. Soc. **109**, 4193 (1987).
[20] G. N. A. van Veen, K. A. Mohamed, T. Baller, and A. E. de Vries, Chem. Phys. **80**, 113 (1983).
[21] H. Okabe, *Photochemistry of Small Molecules* (Wiley–Interscience, New York, 1978).
[22] K. P. Huber and G. Herzberg, *Molecular Spectra and Molecular Structure. IV. Constants of Diatomic Molecules* (Van Nostrand Reinhold, New York, 1979).
[23] P. J. Chantry, J. Chem. Phys. **55**, 2746 (1971).
[24] W. J. van der Zande, R. Zhang, R. N. Zare, K. G. McKendrick, and J. J. Valentini, J. Phys. Chem. **95**, 8205 (1991).
[25] T. H. Dunning, Jr. and P. J. Hay, in *Methods of Electronic Structure Theory*, edited by H. F. Schaefer III (Plenum, New York, 1977), Chap. 1.
[26] S. Huzinaga, J. Chem. Phys. **42**, 1293 (1965).
[27] T. H. Dunning, Jr., J. Chem. Phys. **55**, 716 (1971).
[28] R. Krishnan, M. J. Frisch, and J. A. Pople, J. Chem. Phys. **72**, 4244 (1980).
[29] GAUSSIAN 92, Revision B, M. J. Frisch, G. W. Trucks, M. Head-Gordon, P. M. W. Gill, M. W. Wong, J. B. Foresman, B. G. Johnson, H. B. Schlegel, M. A. Robb, E. S. Replogle, R. Gomperts, J. L. Andres, K. Raghavachari, J. S. Binkley, C. Gonzalez, R. L. Martin, D. J. Fox, D. J. Defrees, J. Baker, J. J. P. Stewart, and J. A. Pople (Gaussian, Pittsburgh, PA, 1992).
[30] H. B. Schlegel, J. Chem. Phys. **84**, 4530 (1986).
[31] P. J. Knowles, J. S. Andrews, R. D. Amos, N. C. Handy, and J. A. Pople, Chem. Phys. Lett. **186**, 130 (1991).
[32] J. L. Chidsey and D. R. Crosley, J. Quant. Spectrosc. Radiat. Transfer **23**, 187 (1980).
[33] P. W. Fairchild, G. R. Smith, D. R. Crosley, and J. B. Jeffries, Chem. Phys. Lett. **107**, 181 (1984).
[34] W. A. Goddard III, *Nature of the Chemical Bond* (California Institute of Technology, Pasadena, 1983).
[35] R. D. Levine and J. L. Kinsey, in *Atom–Molecule Collision Theory*, edited by R. B. Bernstein (Plenum, New York, 1979), p. 693.
[36] R. D. Levine and R. B. Bernstein, *Chemical Reactivity and Molecular Reaction Dynamics* (Oxford, New York, 1983).
[37] G. Herzberg, *Molecular Spectra and Molecular Structure. II. Infrared and Raman Spectra of Polyatomic Molecules* (Van Nostrand Reinhold, New York, 1945).
[38] R. G. Azrak and E. R. Wilson, J. Chem. Phys. **52**, 5299 (1970).